Highly Active and Durable Bimetallic $CoMnO_x$ Catalyst Supported on Carbon Nanofibers for Peroxymonosulfate Activation toward Water Treatment

Siyu Ren, Yue Zhang, Linfeng Zhang, Xiaofeng Lu*

Alan G. MacDiarmid Institute, College of Chemistry, Jilin University, 2699 Qianjin Street, Changchun 130012, P. R. China.

Email: xflu@jlu.edu.cn (X. Lu)

*Corresponding author.

Text S1. Materials

Polyacrylonitrile (PAN, M_w=150 000), potassium peroxymonosulfate (PMS), cobalt nitrate hexahydrate ($Co(NO_3)_2$•$6H_2O$), humic acid (HA) and 2,2,6,6-teramethyl-4-piperidine (TEMP) were purchased from Sigma-Aldrich. Methyl blue (MB), ethanol (EtOH), potassium permanganate ($KMnO_4$), and Rhodamine (RhB) were supplied by Sinopharm Chemical Reagent Co., Ltd. Orange II sodium salt (Orange II), Levofloxacin (LEVO), L-histidine (L-His), furfuryl alcohol (FFA) were available from Aladdin. 5,5-dimethyl-pyrroline-N-oxide (DMPO) (97%) was obtained from Shanghai Macklin Biochemical Technology Co., Ltd. N, N-Dimethylformamide (DMF) was bought from Tianjin Tian tai Fine Chemical Co., Ltd. Tert-butanol (TBA) was sourced form Tianjin Yongsheng Superfine Chemical Industry Co., Ltd. Methyl violet (MV) was procured from Beijing Chemical Works. All of the chemical reagents were used without further purification.

Test S2. Synthesis of catalysts

Synthesis of CNFs

A homogeneous polymeric solution (9 wt%) was formulated by dissolving 0.5 g of PAN powder in 5.25 mL of DMF under continuous magnetic stirring at ambient temperature. The electrospinning process was conducted using a precision syringe pump system, with a distance of 15 cm between the needle of the syringe pump and the grounded collector. A flow rate for the electrospinning solution is 1.5 mL h^{-1} and the applied voltage is fixed as 16 kV. Then the resultant PAN nanofiber mat underwent a pre-oxidation at 240 °C for 2 h in air and subsequent carbonization process at 800 °C for 2 h under an Ar atmosphere, finally yielding a free-standing CNFs membrane.

Synthesis of CNFs@$CoMnO_x$

The CNFs@$CoMnO_x$ was fabricated via a co-deposition strategy. Initially, 10 mg of CNFs were ultrasonically dispersed in 10 mL of $Co(NO_3)_2 \cdot 6H_2O$ aqueous solutions (0.2 mM), forming homogeneous suspensions. Subsequently, 10 mL of $KMnO_4$ aqueous solution (0.75 mg mL^{-1}) was introduced into the mixture under continuous magnetic stirring at ambient temperature. Following 12 h of reaction, the product was collected via centrifugation and subjected to triple washing cycles with deionized water to eliminate ionic residues. The resulting precipitate was freeze-dried under vacuum for 12 h, yielding CNFs@$CoMnO_x$-precursor composite. After that, the thermal annealing process was conducted in a tubular furnace under continuous Ar atmosphere, where the sample was heated to 500 °C at a controlled heating rate of 2 °C min^{-1} and held isothermally for 2 h, yielding the final black CNFs@$CoMnO_x$-500 product. For comparison, control samples of CNFs@MnO_x-500 and CNF@CoO_x-500 were prepared separately under identical conditions only the addition of only single precursor. Furthermore, the annealing temperature is also optimized by changing to 400 °C and 600 °C, and the corresponding samples are denoted as CNFs@$CoMnO_x$-400 and CNFs@$CoMnO_x$-600, respectively.

Text S3. Characterization and analysis methods

The morphological features of the prepared catalysts were characterized using field emission scanning electron microscopy (FESEM, Nova NanoSEM 450 and ThermoFisher Scientific) and transmission electron microscopy (TEM, JEM-2100). High–resolution TEM (HRTEM) was performed on FEI Tecnai G2 F20 instrument. X-ray diffractometer (XRD) was carried out on PAN-alytical B.V. Empyrean and Raman measurement was conducted on alpha300R, WITec. Surface chemical states were examined via X-ray photoelectron spectroscopy (XPS, Thermo Scientific ESCALAB250). Ultraviolet-visible (UV-vis) spectrophotometric analysis (Shimadzu UV-2501) was used to monitor the degradation kinetics. Reactive oxygen species (ROS) generation was verified by electron paramagnetic resonance (EPR) spectroscopy (BRUKER E500). Degradation intermediates were identified using high-performance liquid chromatography mass spectrometer (HPLC-MS, BRUKER micrOTOF-QII).

Text S4. Catalytic degradation procedure and analytical methods

All degradation experiments were conducted in 50 mL beaker at 25 ºC (±1ºC) and the reaction system comprises of 25 mL aqueous solution without buffer addition to eliminate potential interference with reactive oxygen species. The solution pH was controlled through the addition of

hydrochloric acid (HCl) or sodium hydroxide (NaOH). The process commenced with simultaneous introduction of PMS and catalyst into the solution containing RhB contaminant under magnetic stirring. Then a periodic withdrawal of 700 μL of the above solution was mixed with 350 μL of EtOH and 20 μL of L-His (150 mM) in a centrifuge tube to terminate the catalytic reaction. After filtration through a 0.22 μm polyethersulfone (PES) membrane to remove the catalyst, the reaction system was monitored by UV-vis spectrophotometer. Reaction kinetics were quantitatively analyzed through construction of time-dependent C/C_0 profiles derived from contaminant concentration measurements at progressive degradation stages. Triplicate experimental replicates were performed under identical conditions to ensure methodological accuracy.

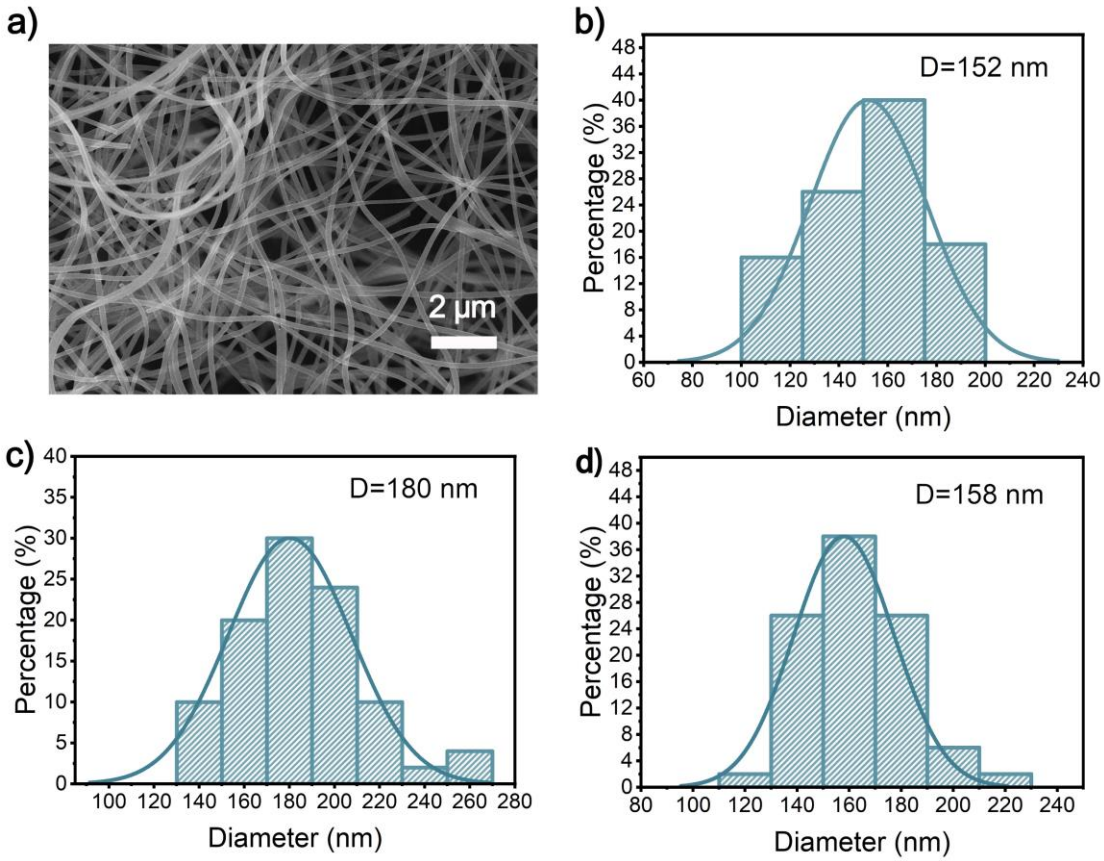

Fig. S1. (a) FESEM image of CNFs. Diameter distribution of b) CNFs, c) CNFs@$CoMnO_x$-precursor sample and d) CNFs@$CoMnO_x$-500 sample.

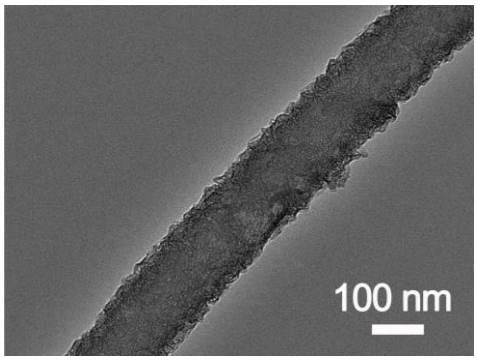

Fig. S2. TEM image of CNFs@$CoMnO_x$-precursor.

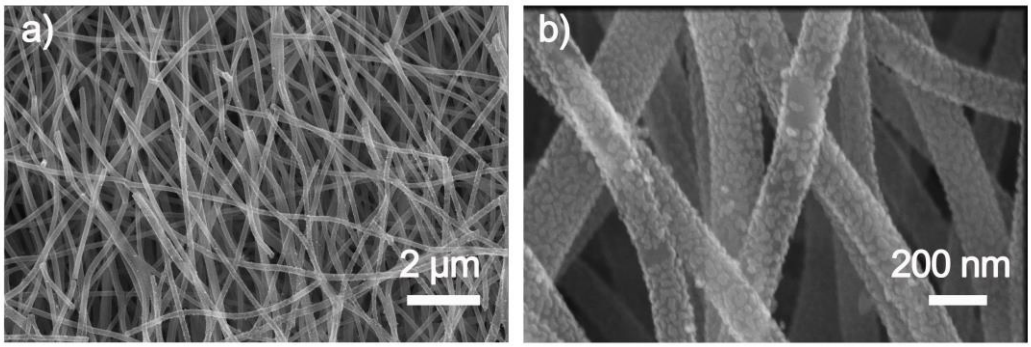

Fig. S3. (a, b) FESEM image of CNFs@$CoMnO_x$-400.

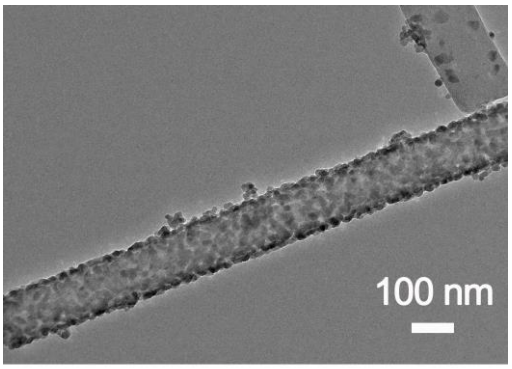

Fig. S4. TEM image of CNFs@$CoMnO_x$-400.

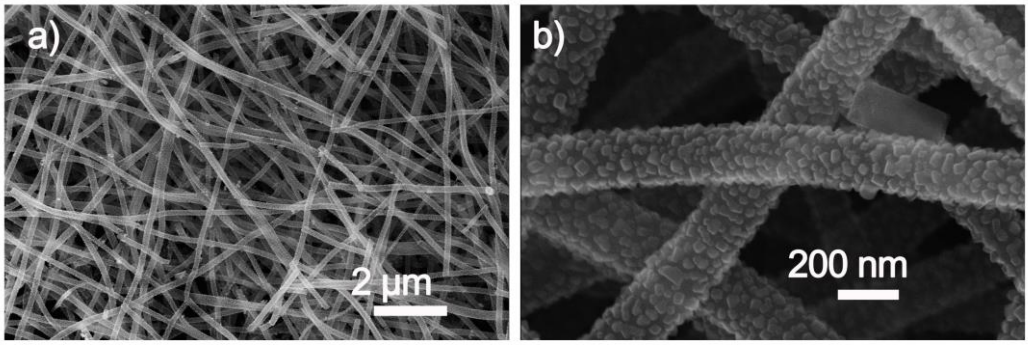

Fig. S5. (a,b) FESEM image of CNFs@$CoMnO_x$-600.

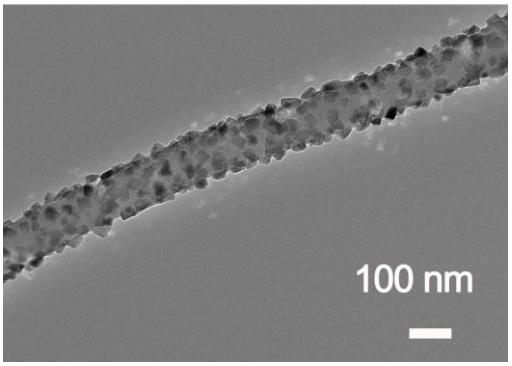

Fig. S6. TEM image of CNFs@$CoMnO_x$-600.

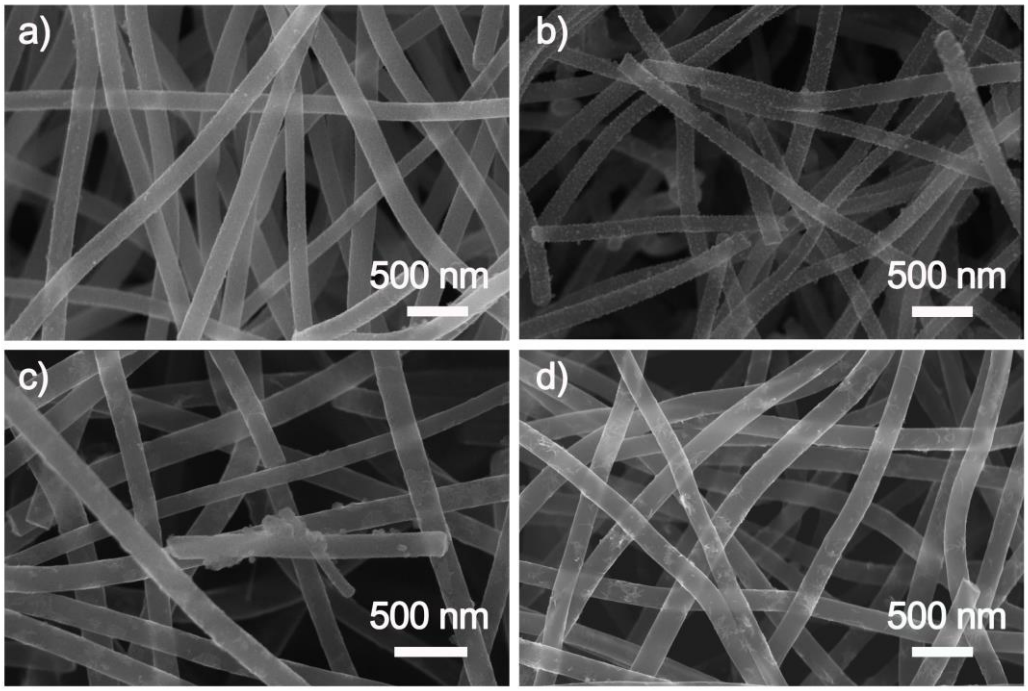

Fig. S7. (a) SEM image of CNFs@MnO_x precursor, (b) SEM image of CNFs@MnO_x-500, (c) SEM image of CNFs@CoO_x precursor, (d) SEM image of CNFs@CoO_x-500.

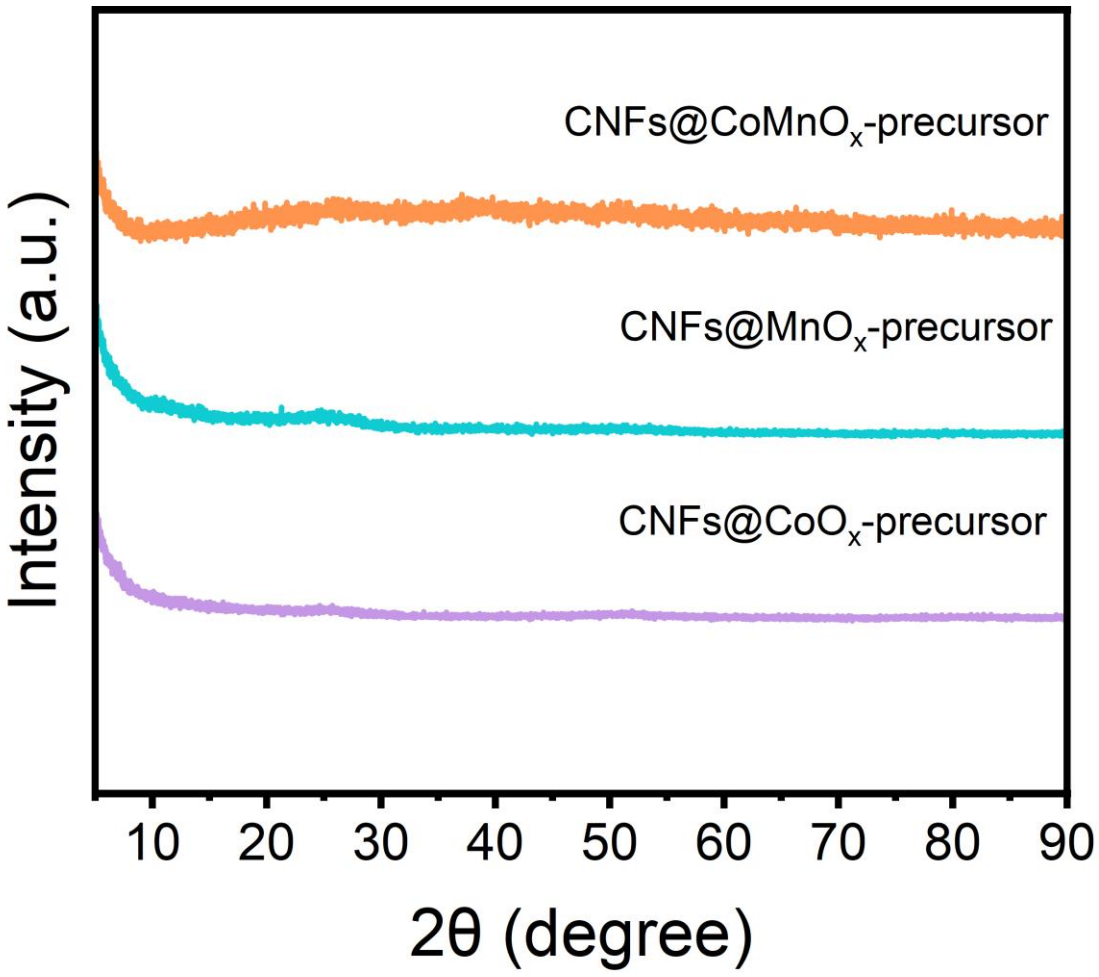

Fig. S8. XRD patterns of CNFs@CoMnO$_x$-precursor, CNFs@MnO$_x$-precursor and CNFs@CoO$_x$-precursor materials (without annealing).

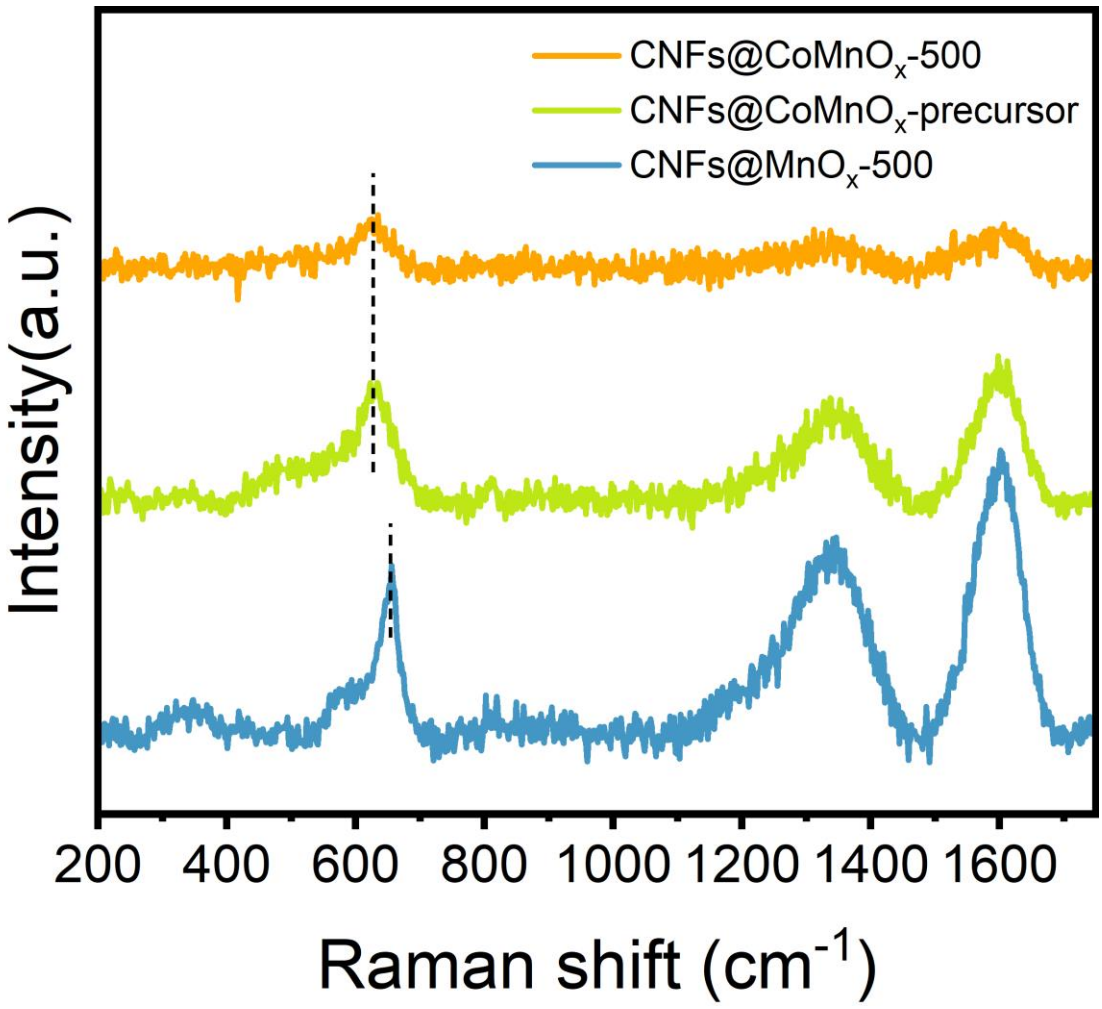

Fig. S9. Raman spectra of CNFs@MnO_x-500, CNFs@$CoMnO_x$-precursor and CNFs@$CoMnO_x$-500.

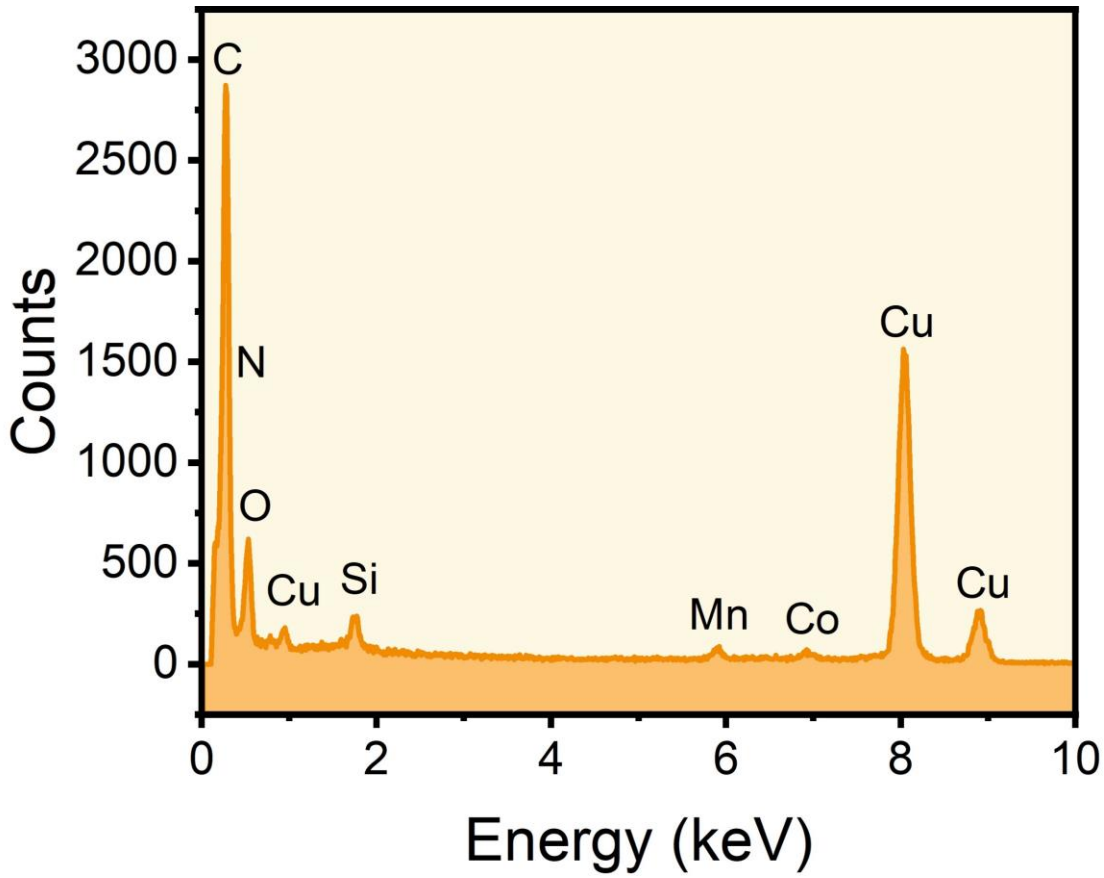

Fig. S10. EDX spectrum of CNFs@$CoMnO_x$-500 sample.

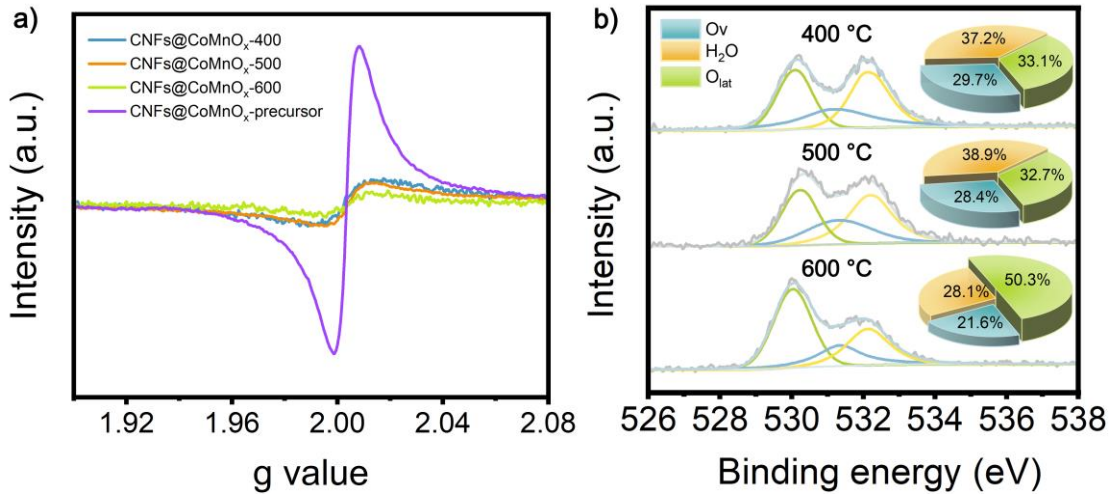

Fig. S11. (a) EPR spectra of different materials; (b) XPS spectra of O 1s in different materials

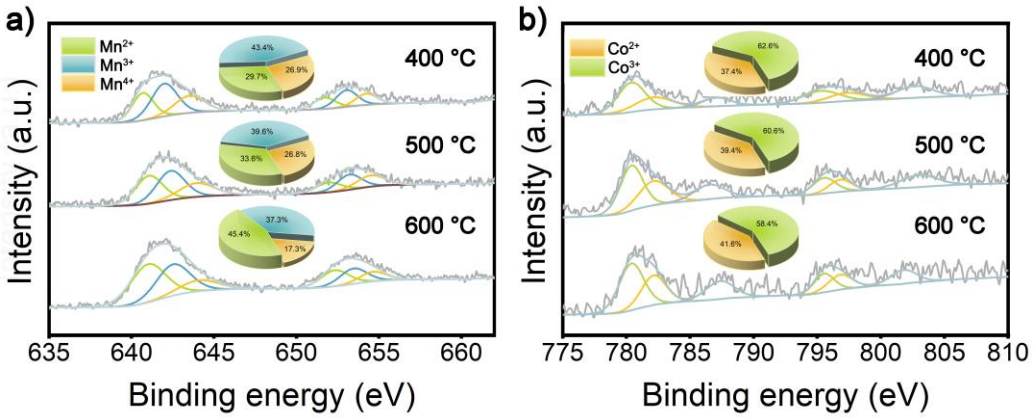

Fig. S12. XPS spectra of CNFs@CoMnO_x-500: (a) Mn 2p, (b) Co 2p.

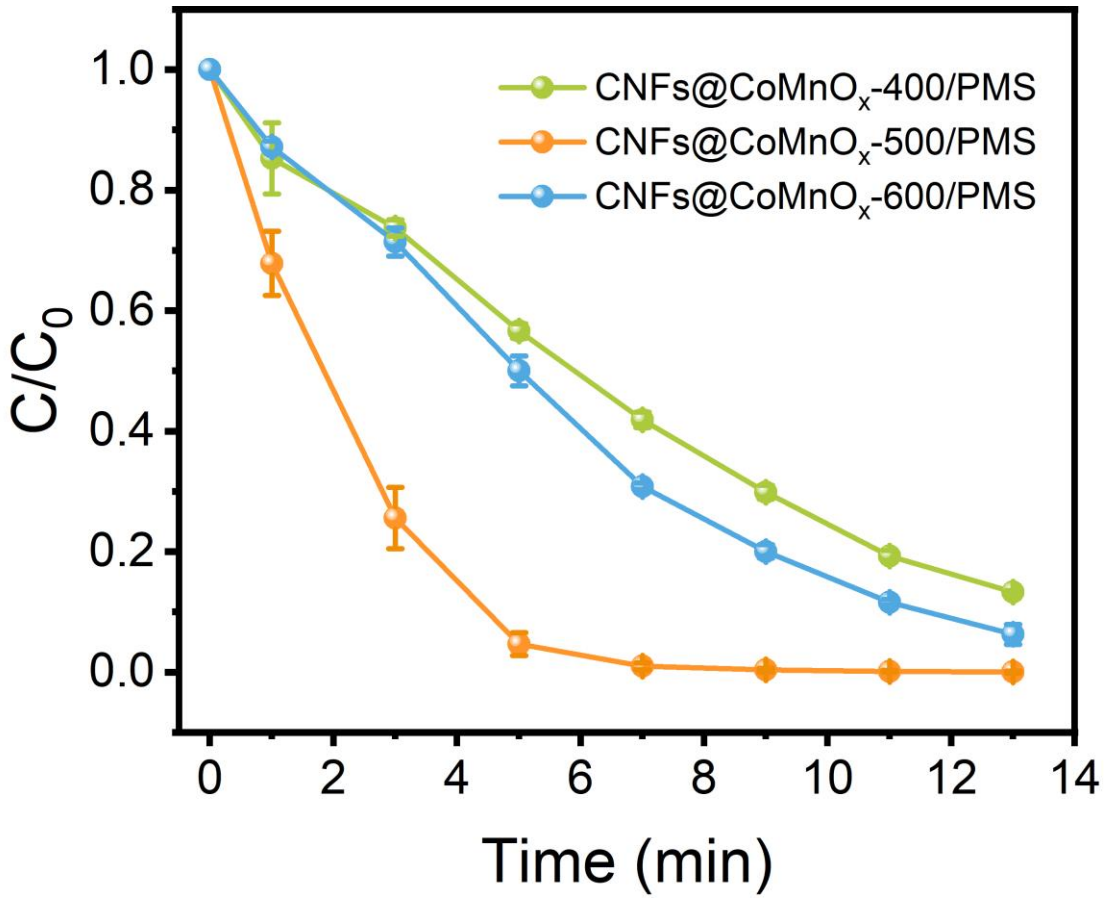

Fig. S13. RhB degradation curves in different systems.

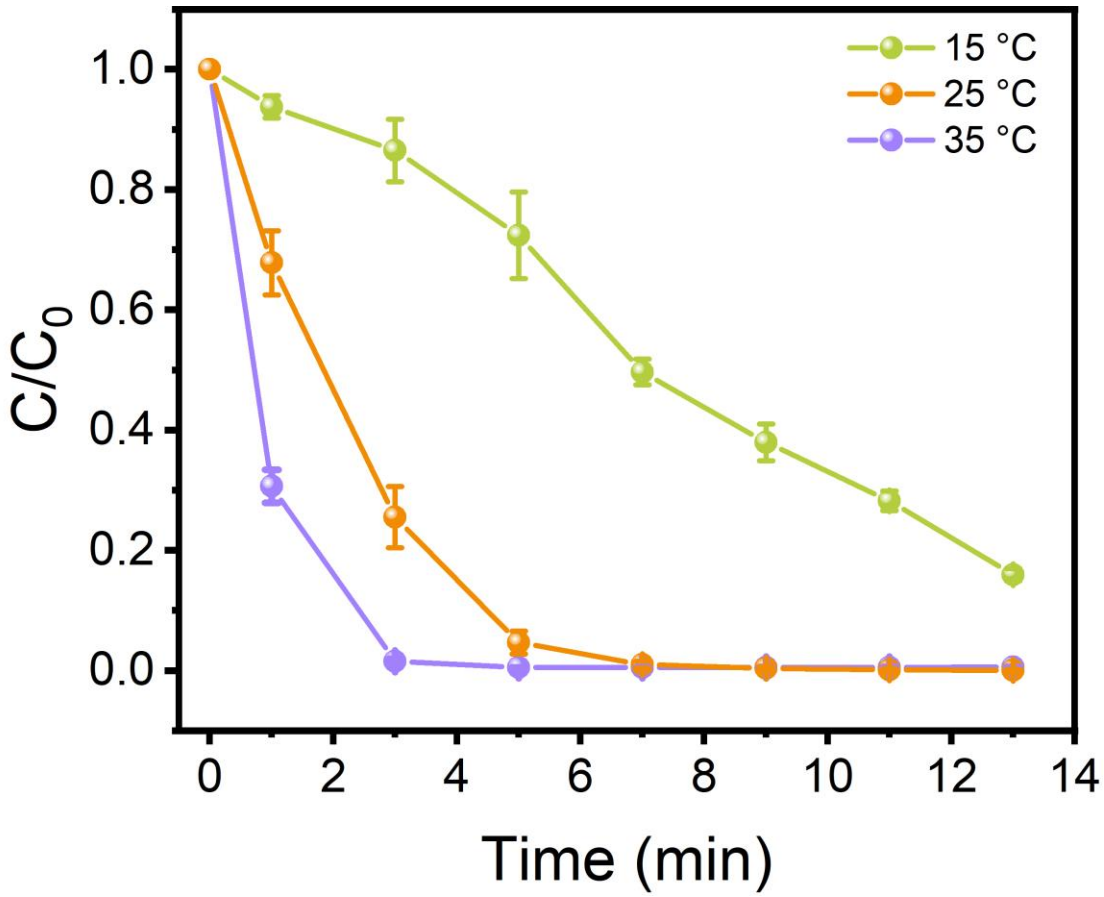

Fig. S14 The effect of reaction temperature.

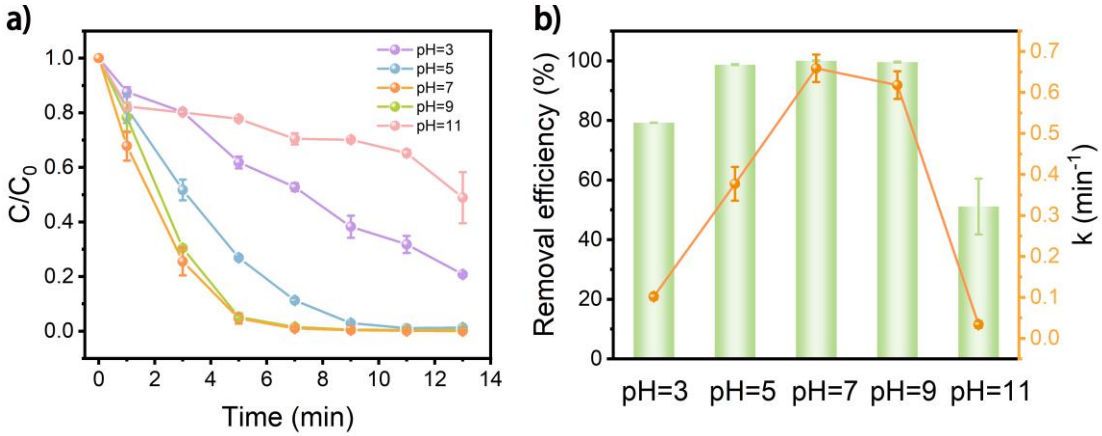

Fig. S15 (a) RhB degradation curves, (b) histogram of first-order kinetic constant values in varied pH reaction systems.

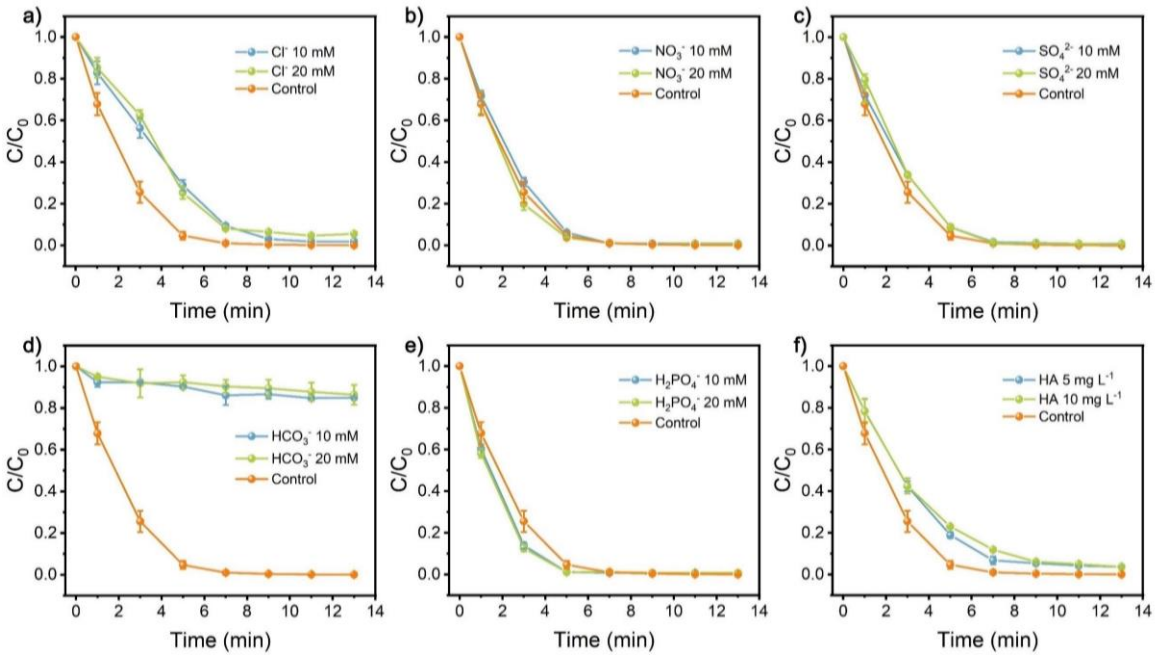

Fig. S16. Influence of anions (a) Cl^{-}, (b) NO_3^{-}, (c) SO_4^{2-}, (d) HCO_3^{-}, (e) $H_2PO_4^{-}$ and organic substance of (f) HA on RhB degradation.

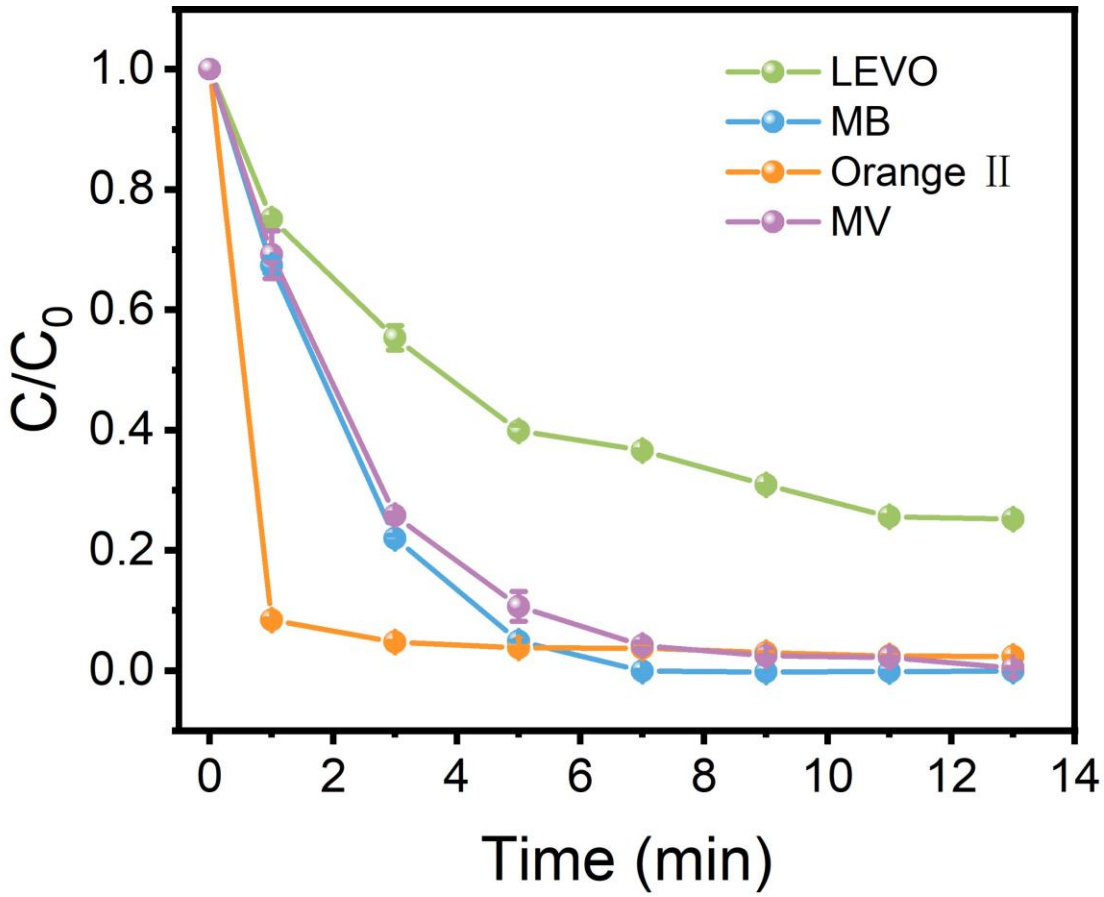

Fig. S17. Catalytic performance of catalysts as a function of different contaminants.

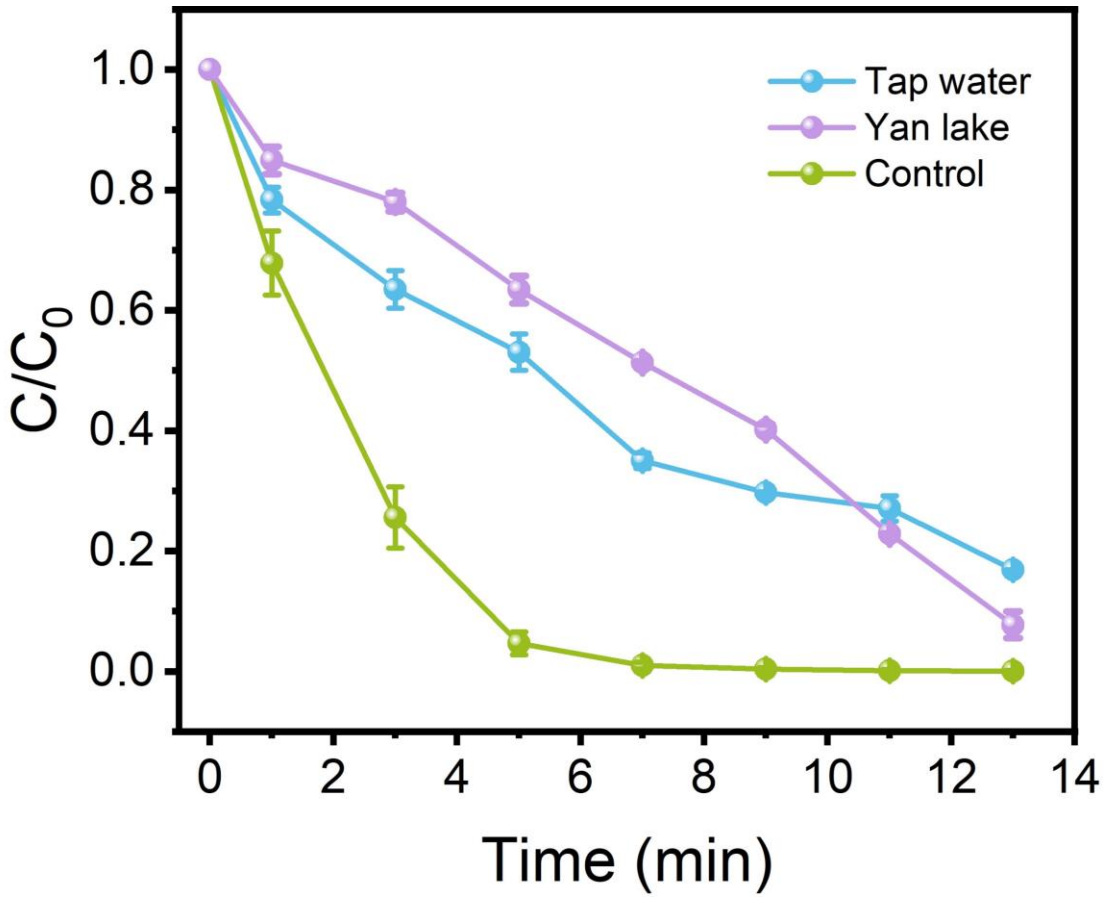

Fig. S18. The catalytic performance for RhB degradation in the real water systems.

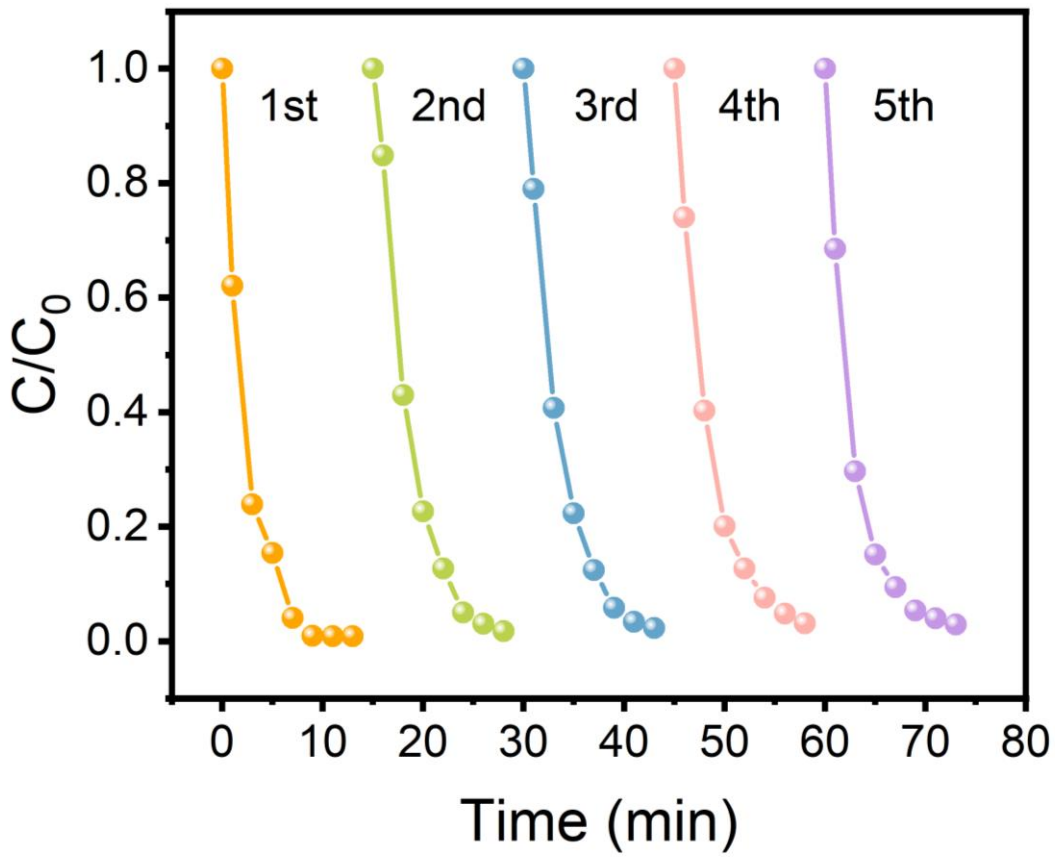

Fig. S19. Recyclability test for RhB degradation.

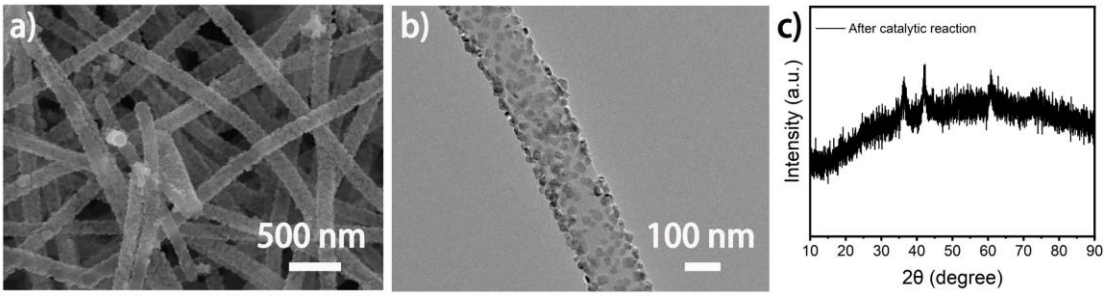

Fig. S20. (a) SEM, (b) TEM image and (c) XRD pattern of CNFs@$CoMnO_x$-500 after catalytic reaction.

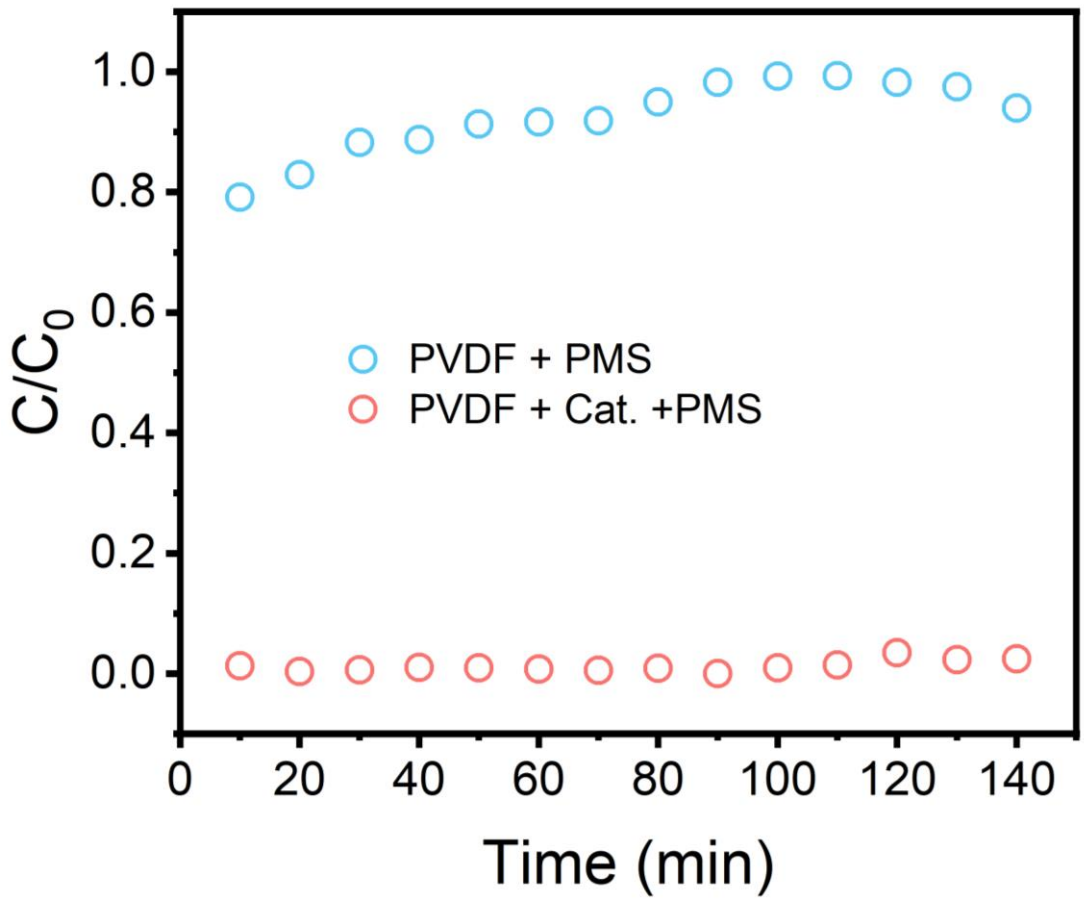

Fig. S21. RhB removal efficiency from CNFs@$CoMnO_x$-500-based membrane system.

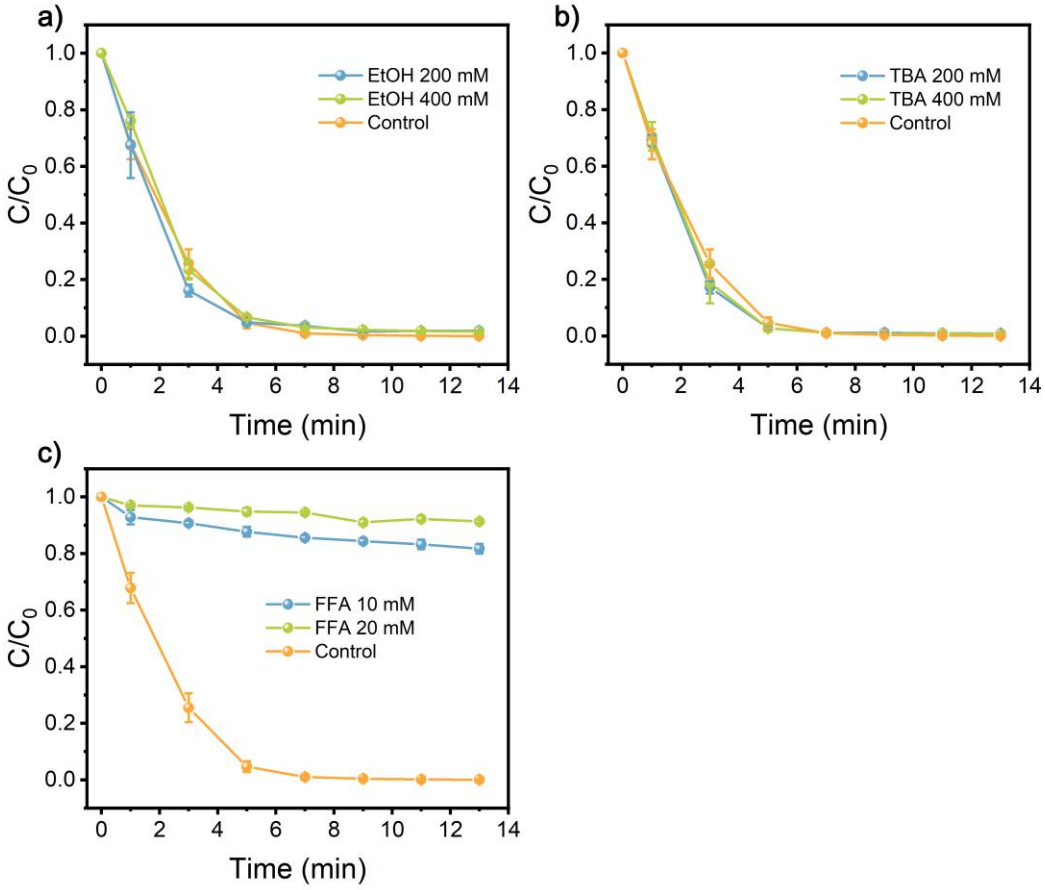

Fig. S22. The quenching tests of CNFs@$CoMnO_x$-500/PMS system with diverse quenchers (a) EtOH, (b) TBA and (c) FFA.

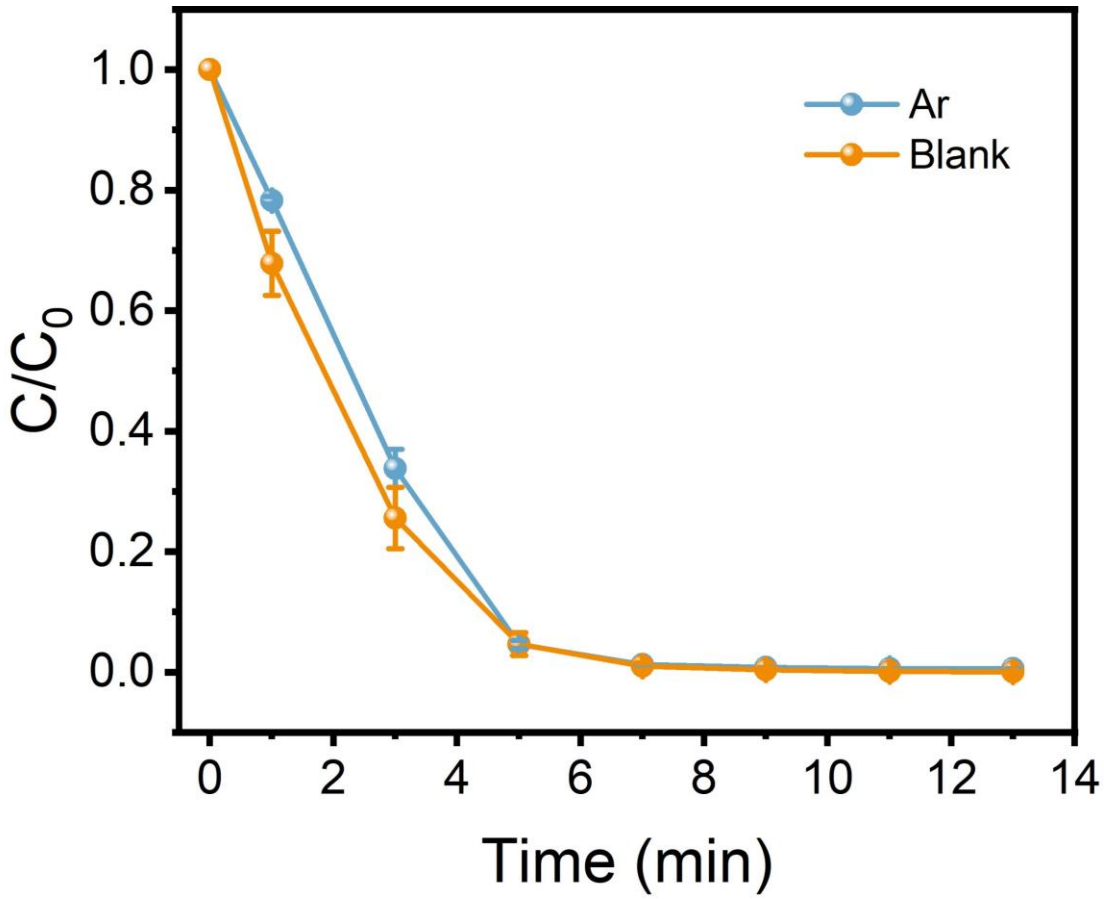

Fig. S23. Effect of Ar-saturated solutions on RhB degradation in CNFs@$CoMnO_x$-500/PMS system.

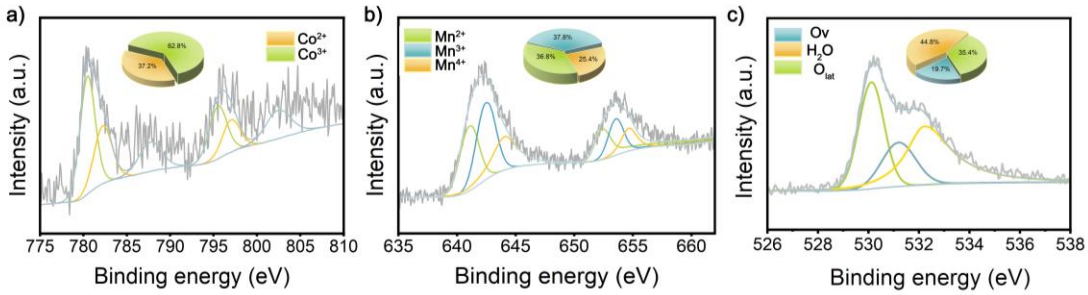

Fig. S24.XPS spectra of post CNFs@CoMnO_x-500: (a) Co 2p, (b) Mn 2p, (c) O 1s.

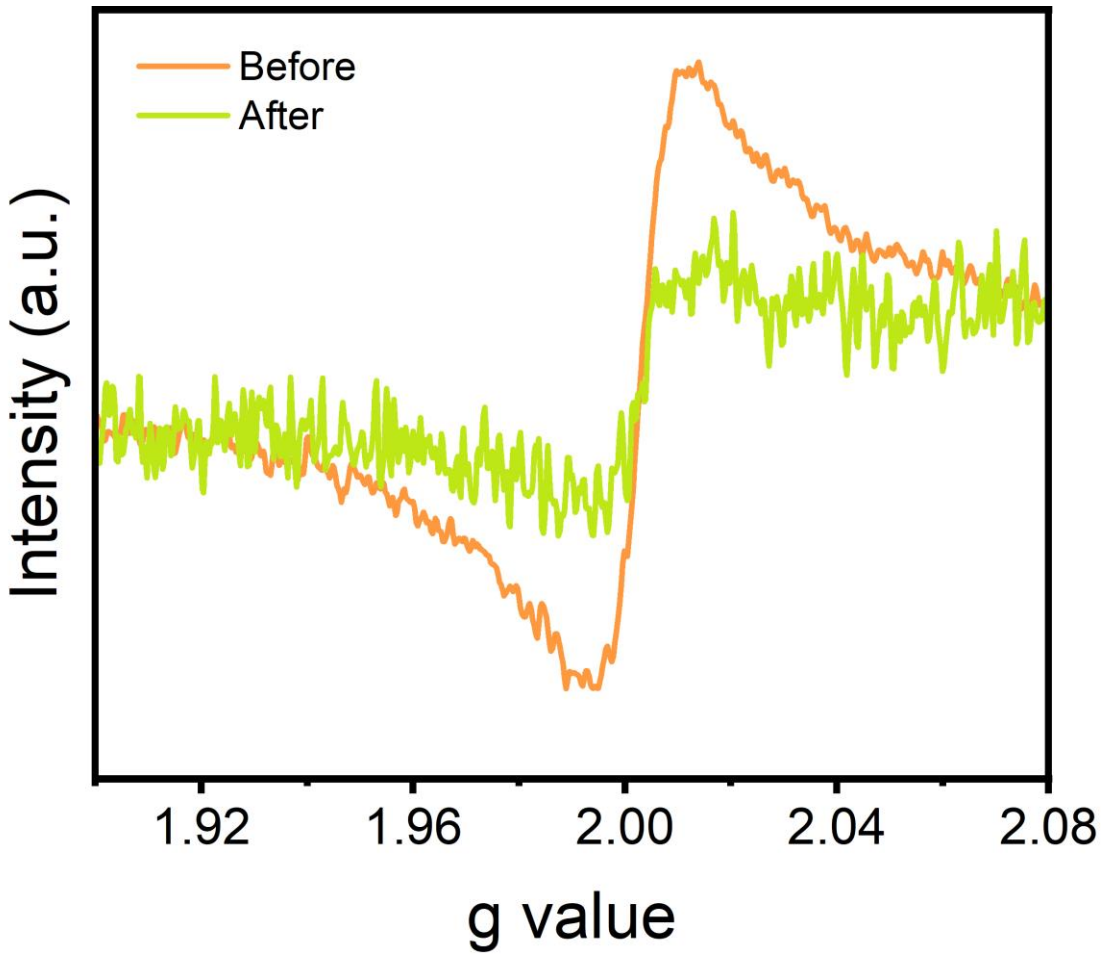

Fig. S25. EPR of CNFs@$CoMnO_x$-500 after catalytic reaction.

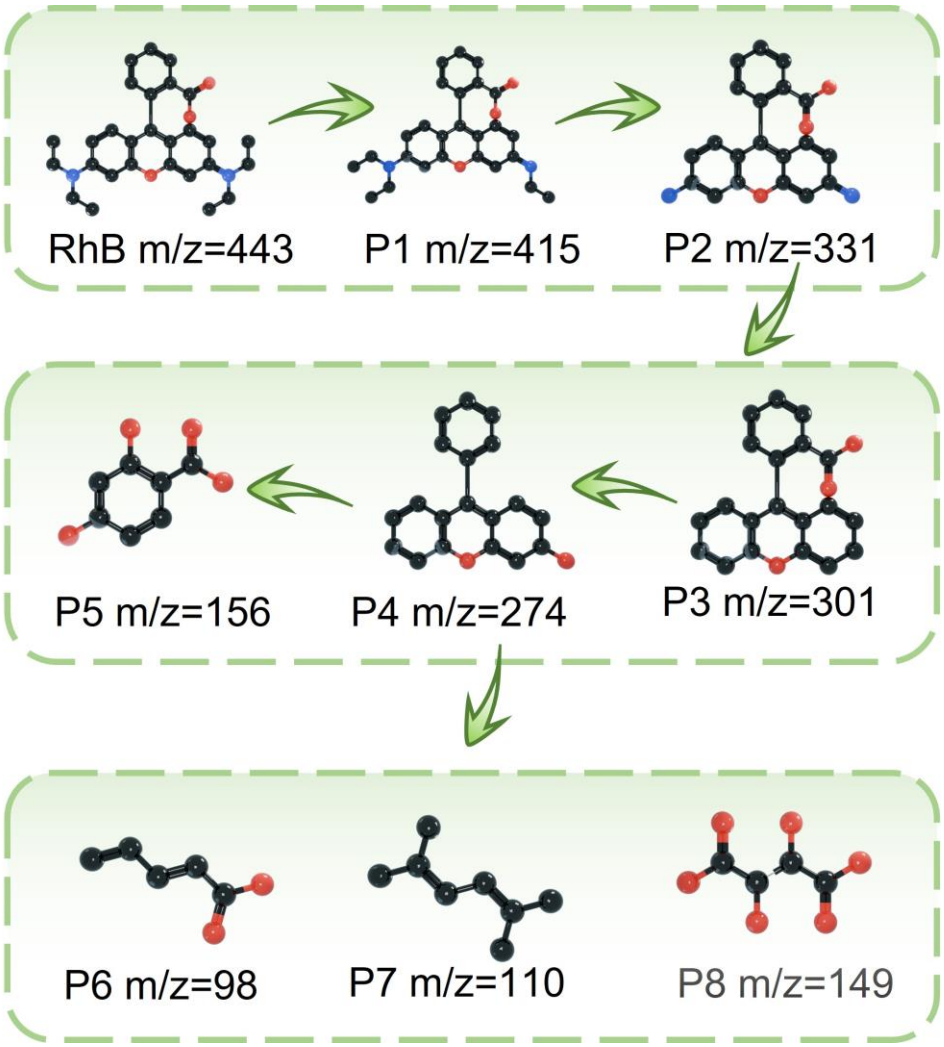

Fig. S26. Proposed pathways for RhB degradation in the CNFs@CoMnOx-500/PMS system.

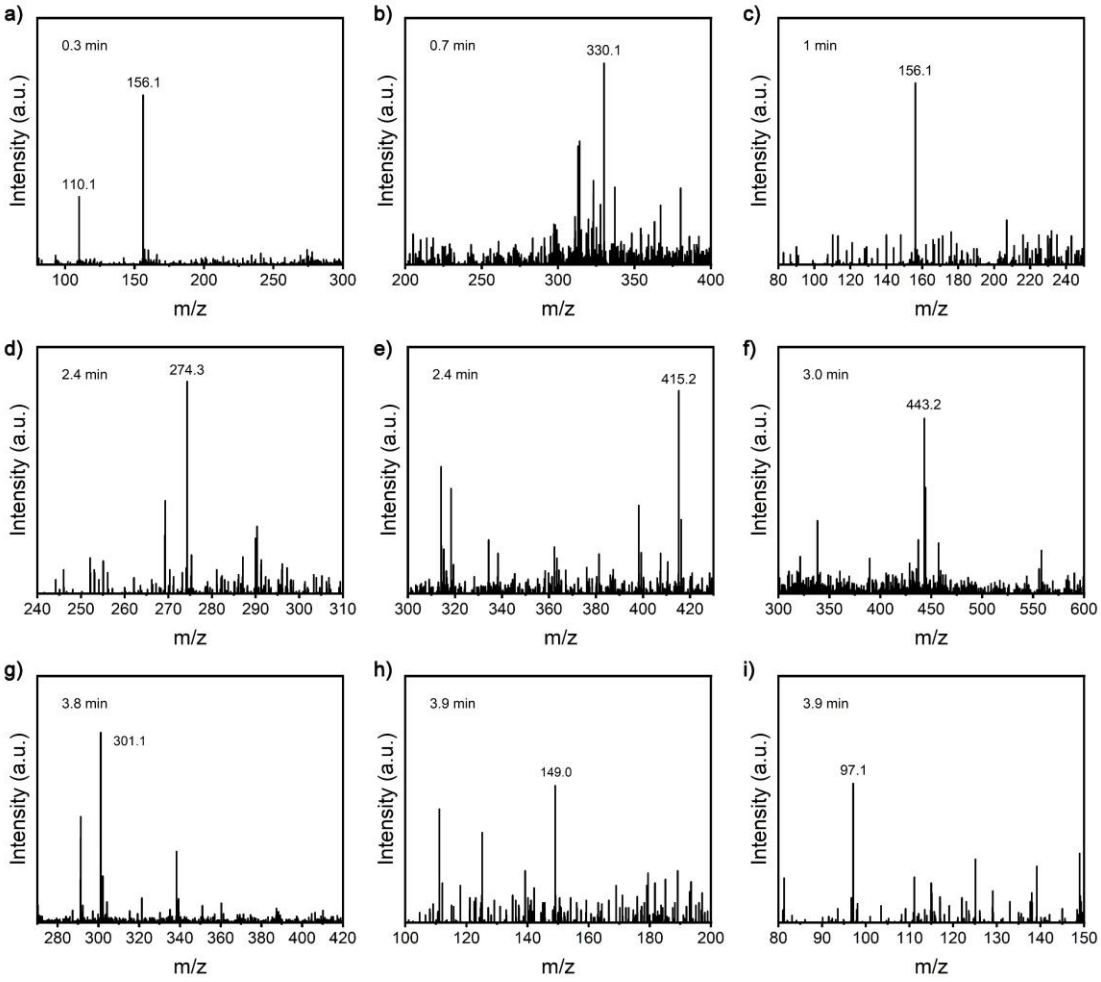

Fig. S27. LC-MS spectra of RhB decomposition in CNFs@$CoMnO_x$-500/PMS system.

Table S1. Comparison of the catalytic performance for RhB removal by CNFs@$CoMnO_x$−500 with some reported catalysts.

Catalysts	[catalyst] (g L^{-1})	[PMS] (g L^{-1})	[RhB] (g L^{-1})	[PMS]/[RhB]	k (min^{-1})	
CNFs@$CoMnO_x$ -500	0.04	0.20	0.02	10	0.659	This work
NCM-650	0.5	0.307	0.02	15.35	0.179	[1]
$CoFe_2O_4$-CV	0.1	0.154	0.1	1.54	0.401	[2]
$CoFe_2O_4$@ATP–BC	0.1	0.307	0.02	15.35	0.303	[3]
α-MnO_2	0.2	0.05	0.02	2.5	0.092	[4]
$CoFe_2O_4$@CB	0.4	0.301	0.04	7.53	0.070	[5]
Fe_3O_4-MnO_2	0.3	0.3	0.02	15	0.264	[6]
H-CoFe PBA@PPy	0.05	0.2	0.02	10	0.385	[7]
$CoTiO_3$@Co_3O_4	0.5	0.307	0.05	6.14	0.199	[8]
1NOC-Mn_3O_4	0.2	0.3	0.01	40	0.101	[9]
Cu-doped $CoFe_2O_4$	0.5	0.614	0.010	61.4	0.551	[10]

References

[1] Y. Zhao, H. Wang, J. Ji, X. Li, X. Yuan, A. Duan, X. Guan, L. Jiang and Y. Li, *J. Colloid Interface Sci*., 2022, **626**, 564-580.

[2] Z. Jin, X. Zhao, M. Zhang, Y. Li, J. Guo, Y. Lan and C. Chen, *J. Water Process. Eng*., 2024, **60**, 105221.

[3] Y. Pan, F. Meng, J. Bai, B. Song and Q. Cao, *J. Environ. Chem. Eng.,* 2024, **12**, 112579.

[4] J. Li, Q. Shi, M. Sun, J. Liu, R. Zhao, J, Chen, X. Wang, Y. Liu, W. Gong, P. Liu and K. Chen, *Molecules* 2023, **28**, 4388.

[5] B. E. Allaoui, H. Benzeid, N. Zari, A. Qaiss and R. Bouhfid, *Int. J. Biol. Macromol*., 2024, **259**, 128893.

[6] Q. Shi, S. Pu, X. Yang, P. Wang, B. Tang and B. Lai, *Chin. Chem. Lett.,* 2022, **33**, 2129-2133.

[7] N. Song, S. Ren, Y. Zhang, C. Wang and X. Lu, *Adv. Funct. Mater.,* 2022, **32**, 2204751.

[8] H. Li, Q. Gao, G. Wang, B. Han, K. Xia and C. Zhou, *Appl. Surf. Sci.,* 2021, **536**, 147787.

[9] Y. Xu, Y. Li, J. Feng, C. Wang, C. Zhang, Y. Wang and X. Cheng, *Chin. Chem. Lett.,* 2024, **35**, 108838.

[10] Y. Mo and X. Zhang, *J. Environ. Sci.,* 2024, **137**, 382-394.